The International Journal of Advanced Manufacturing Technology

The International Journal of Advanced Manufacturing Technology bridges the gap between pure research journals and the more practical publications on advanced manufacturing and systems. It therefore provides an outstanding forum for papers covering applications-based research topics relevant to manufacturing processes, machines and process integration. — show all

ORIGINAL ARTICLE

Analysis on grain growth of SS316L induced by plasma cutting process using probabilistic FEM with experimental verification

Mohd Shahar Sulaiman[1,2] · Yupiter H. P. Manurung[1,2] · Baohua Chang[3] · Mohd Shahriman Adenan[1,2] · Qairul Najmi Enseri[2] · Norasiah Muhammad[4] · Hui Leng Choo[5,6] · Muhd Faiz Mat[1,2] · Birgit Awiszus[7] · Andre Haelsig[8] · Salina Saidin[9] · Yusuf Olanrewaju Busari[1,2,10]

Abstract

This fundamental research was conducted to predict the grain size of austenitic stainless-steel after plasma cutting process using experiment and non-linear probabilistic numerical computation with self-developed algorithm which was written and compiled using Fortran-based subroutines and utility routines available in commercial FEM software. For grain modelling, the non-linear numerical programming codes consisted of fourth-order Runge–Kutta method for solving ordinary differential equation of grain growth formula with major parameters such as initial grain size, activation energy, and kinetic constant which were measured by using dilatometer on specimen samples at various temperatures and holding times. In order to replicate the actual thermal cutting process, customized conical heat source model was developed and employed. The probabilistic approach in numerical computation was executed using Monte Carlo method by setting major process parameter of input power based on normal distribution with defined mean and standard deviation which were randomized following linear congruential generator and Box-Muller algorithm. This comprehensive numerical computation based on deterministic and probabilistic FEM was established using nonlinear thermomechanical method with hexahedral element type including finer mesh on cutting section and coarser at base plate. For verification purpose, a series of experiments using fully automated system was carried out on SS316L plate with 4-mm thickness. From the analysis of results, acceptable discrepancy was achieved in grain size prediction obtained between numerical methods and experiment with the error percentage of up to 9.2% and 14.5% for probabilistic and deterministic analyses respectively.

Keywords Deterministic · Probabilistic · Grain size · Numerical Computation · SS316L

✉ Yupiter H. P. Manurung
yupiter.manurung@uitm.edu.my

1 Smart Manufacturing Research Institute (SMRI), Universiti Teknologi MARA (UiTM), Shah Alam, Malaysia

2 School of Mechanical Engineering, College of Engineering, Universiti Teknologi MARA (UiTM), Shah Alam, Malaysia

3 Institute of Materials Processing Equipment and Automation, Tsinghua University, Beijing, China

4 Mechanical Engineering Department, Politeknik Premier Sultan Salahuddin Abdul Aziz Shah, Shah Alam, Malaysia

5 School of Engineering, Taylor's University, Subang Jaya, Malaysia

6 Center for Smart Society 5.0, Additive Manufacturing Cluster, Faculty of Innovation and Technology, Taylor's University, Subang Jaya, Malaysia

7 Professorship of Virtual Production Engineering, Chemnitz University of Technology, Chemnitz, Germany

8 Chair of Welding Engineering, Chemnitz University of Technology, Chemnitz, Germany

9 Nusantara Technologies Sdn Bhd, Shah Alam, Malaysia

10 Materials and Metallurgical Engineering Department, University of Ilorin, Ilorin, Nigeria

1 Introduction

As one of the separating processes, thermal cutting is a very important method in fabrication industry. This process uses concentrated heat to be imposed on a metallic or non-metallic plate, causing the applied part to melt away. Typically, thermal cutting is an exothermal process where less heat is needed for maintaining the burning process. Main thermal cutting processes are flame, plasma arc, and laser cutting [1]. The most extensively utilized thermal cutting process is known as flame cutting due to its low-cost equipment and easy to handle. The flame cutting can be manually applied and also can be easily automated [2]. The flame cutting is also called as oxyfuel gas cutting and oxyacetylene cutting. This process is a thermochemical process that works by initially preheating the material to its ignition temperature which is lower than its melting point, and subsequently, the preheated area is subjected to pure oxygen jet to produce iron oxides which are then blown away by the oxygen jet to generate cut kerf that penetrating through the material. The flame cutting has the capability to produce good quality cutting which can be employed to cut material with the thickness ranging from 5 up to 120 mm [3].

In plasma arc cutting (PAC), the applied part of workpiece material is melted and partially vaporized away by extremely hot plasma gas that is produced through the combination of an arc with inert gas flow or pressurized air. Plasma arc is produced by means of heating the gas with an arc that results into partly ionized which is capable to conduct electricity. More accurate and hotter arc is generated by concentrating the plasma arc through a nozzle that can reach extremely high operating temperature of around 10,000 to 14,000 °C. Fast action of heating the gas when moving along the arc leads to expansion which then accelerates via the nozzle and focuses towards the workpiece. High speed of plasma gas jet is utilized to get rid of the molten materials. Types of gases that are typically used for plasma cutting process consist of air, argon, oxygen, nitrogen, and mixture of argon and hydrogen as well as mixture of nitrogen and hydrogen [4, 5].

Laser cutting is an advanced non-contact thermal cutting process which can avoid effects like tool wear, vibration of machine, and mechanically induced thermal damage [6]. Laser cutting can be used for nearly all types of materials such as metals, non-metals, composites, and ceramics. It has the capability to produce complex shapes and various geometries with the narrow kerf. As stated in [7], instead of mechanical properties, the potential of laser cutting primarily depends on thermal and optical properties. A cut kerf is formed by the action of removing the molten material as the assist gas blows it away where the molten material is produced as a result of locally focused laser beam onto the material.

Numerous thermal analyses have been performed by means of numerical methods. A thermomechanical numerical analysis was conducted on carbon steel material to observe the effects of flame cutting parameters on HAZ (heat affected zone) size [8]. The simulated HAZ size was found to be closer to the actual HAZ size obtained through experiment. The results showed that the increase in cutting speed led to decreasing in HAZ width at the center area. Meanwhile, the increase in ethylene (C_2H_4) flow rate caused the upper HAZ width to increase whereas the increasing flow rate of oxygen caused the widening of the lower HAZ width. Another research on numerical simulation of flame cutting on steel material had been performed in [9]. Referring to this research, a quasi-stationary state model can be used when the flame size is far much smaller than the plate size with straight cutting line. In addition, the quasi-stationary state model was coupled with transport equations to describe the transition of phase based on transient Leblond-Devaux model. A portion of molten material was removed during cutting process resulting in the formation of heat-affected zone (HAZ) in the region around the cut kerf. The HAZ is the area where transitions of phases take place as a result of austenitization. It can be found that the HAZ and kerf widths were reduced when the cutting speed was increased.

In [10], a study on forecasting distribution of temperature induced by thermal cutting on Inconel 718 was carried out. The numerical computation was made based on thermo-mechanical analysis using temperature-dependent properties of material. From the results, it was found that the estimated temperature distribution was in good agreement with the actual temperature measurement. The trend of temperature provided by 2-mm thickness specimen was slightly higher than that of 1-mm thickness specimen. According to [11], arc cutting and arc welding processes were based on the similar basic principles in which some parts of materials were removed in cutting process, whereas some filler materials in welding process were normally added up to the base material to form the joint. Research on numerical simulation of multipassed welding distortion induced in combined joint by gas metal arc welding (GMAW) was conducted in [12]. Commercial software SYSWELD was used for predicting the distortion which was implemented through thermo-mechanical plus metallurgical analysis. Plasticity criterion calculated using isotropic strain hardening caused by non-cyclic loading was defined for mechanical analysis whereas constitutive equation formulated by Leblond was defined for metallurgical history consideration. The results revealed that the angular distortion predicted through 2D analysis showed reasonable agreement with the prediction using 3D analysis. The 2D analysis has an advantage over 3D analysis in terms of computational time in which the 2D analysis was completed in much faster time compared to 3D analysis. A study on residual stresses produced in pipe girth weld of

316 stainless steel was carried out [13]. The residual stress prediction was computed through thermo-elastic–plastic mechanical analysis. The numerical analysis was implemented by means of three different hardening models comprising of isotropic, kinematic, and mixed hardening models which were computed depending on flow curves, bilinear-Ziegler rule, and Lemaitre-Chaboche model respectively. Comparing to experimental measurements, good predictions of axial stresses and hoop stresses were obtained through isotropic hardening model while the mixed hardening model provided the best prediction for hoop stresses. On the other hand, the numerical analysis via kinematic hardening model underestimated both predictions of axial and hoop stresses.

It is well known that finite element analysis is implemented typically based on deterministic method. However, in the deterministic analysis, even though all the criteria have been taken into account, it still leads to limited description of the characteristics of a system [14]. The research on complex phenomena like dynamic loading, inherent randomness of material, lack of data, and human error has always come up with various sources of uncertainty. In order to enhance the classical FEM, other new numerical approaches have been added up in the analysis which considered the uncertainty of parameters. This new type of analysis is identified as a stochastic finite element method [15], a random finite element method [16], and a probabilistic finite element method [17]. In addition, to enable the variation of stochastic scenarios, random fields are applied in the analysis for characterizing the nature of stochastic in the system. To determine the effects of random variations, the statistical information of the response variables is assessed by including the calculation on the probability of system output. In [18], research was conducted on optimization of laser cutting parameters via probabilistic FEM. The process parameters involved in the CO_2 laser cutting of stainless steel 304 comprised of travel speed, assist gas pressure and focus position, laser power, and kerf taper angle which were connected in the analysis through the implementation of artificial neural network-based mathematical model using Monte Carlo (MC) method. MC method is considered as a common mathematical tool used in numerical simulation for solving numerous problems which are operated by manipulating random numbers in the programming algorithm. The statistical result of kerf taper angle demonstrated good accuracy when compared to experimental measurement. The MC method was found to have the capability to minimize the kerf taper angle by optimizing the laser cutting parameters. Furthermore, an acceptable kerf taper angle was achieved by focusing the laser beam on about two-third of the thickness of material with the application of low assist gas pressure of 9 bar and also combining high cutting speed of 3 m/min with low laser power of 1.6 kW. The optimization through MC simulation could be resolved by generating random numbers that were uniformly distributed in the range between 0 and 1. To fulfill the limitations of parameter values, manipulation of the random numbers was implemented with the purpose to generate uniformly distributed random numbers for each of the laser cutting parameter which was laid within the range of interest that could be accomplished.

A huge number of input parameters are involved in predicting oil and gas reserves and resources particularly in complex projects [19]. The prediction via deterministic method was normally faced with limited capability in order to take the effects of uncertainties such as seismic, petrophysics, and porosity into consideration. Therefore, probabilistic method was preferred because its projection was made by considering a lot of uncertainties which could provide higher confidence levels in evaluation. The advancement in computing technologies would provide better assessments through intensive probabilistic method with artificial intelligence. Due to un-bias results produced by probabilistic method, it was used in predicting the mainstream of reserves and resources which could assist the practitioners to describe the downside and upside of the projects. Based on research in [20], probabilistic and deterministic methods were implemented to evaluate marine pipeline corrosions which could adversely affect the structural integrity. Among the weaknesses produced via deterministic analysis were lack of understanding in importance of various input parameters, lack of understanding in influence of every single failure mechanism, uncertainties in the physical models, as well as variables were not taken into consideration. However, these limitations could be overcome through the implementation of probabilistic analysis. The load and strength variables were fixed in deterministic analysis, whereas these variables were normally distributed in probabilistic analysis. The defect assessment triggered by the corrosion can be estimated through the comparison of calculated failure pressure with the load imposed on the pipeline. As for deterministic method, the assessment can be made where the capability of the pipeline to withstand against the load increased with the increasing value of calculated failure pressure. In probabilistic method, the assessment can be defined by comparing the calculated failure probability with respect to the service time where the pipeline was increasingly susceptible to fail when the failure probability approached the value of 1.0. Through deterministic analysis, the increasing defect length led to decreasing failure pressure and thus lowered the capability of the pipeline to resist against the exerted load. However, in probabilistic analysis, all the approaches showed that the failure probability of pipeline reached the value of 1.0 which indicated towards the pipe failure when its service time closes to 20 years. The evaluation made based on probabilistic method could provide higher reliability on

the aging corroded marine pipeline performance towards its remaining service lifecycle. Through the probabilistic analysis, the current performance of the aging pipeline in service could be better assessed as compared to the result obtained from the deterministic analysis.

Numerous researches on the calculation of grain growth were performed previously especially due to heat-induced processes such as welding process [21–23]. Study on behavior of grain growth using stainless steel material in consequence of cooling rates was conducted in [24]. Calculations of cooling rates were made through numerical analysis using phenomenological model, whereas the microstructural measurements of secondary dendrite arm spacing (SDAS) were conducted on the welded samples using scanning electron microscopy (SEM) for verifying the predicted results. The computed results were in good agreement with the actual measurements, and the grain growth was found to be influenced by the cooling rate in which slower cooling rate would increase the grain size. As stated by research in [25], grain growth in the heat-affected zone (HAZ) of stainless-steel material was hugely depended on the main factors such as maximum temperature, rate of cooling, and a period of staying at high temperature. The grain was greater in size in the area that was undergoing higher maximum temperature when compared to the grain size in the area that was undergoing lower maximum temperature. The changes in temperature throughout heating and cooling cycles would influence the grain size in which the grain growth typically occurs between the temperature of 900 °C and its peak temperature. In addition, particle precipitation and grain boundary migration were also the major factors that could provide great impact on the grain growth in stainless steel material.

Based on reviewed literatures, there were only few attempts in comparative prediction of grain size using probabilistic and deterministic FEM especially for thermal cutting process due to limited numerical software capability to solve the problem by default which leads to the need of comprehensively advanced approaches using subroutines and utility routines. Therefore, in this study, non-linear thermo-mechanical probabilistic computation method based on Monte Carlo using FEM software Marc/Mentat 2016 was employed to model and simulate plasma arc cutting process for predicting the grain growth in 4-mm plate thickness of austenitic stainless steel 316L. A series of experiments were carried out using fully automated system for validating the simulated results. To measure the initial and final grain sizes of the specimen, an advanced system of metallurgical microscope was utilized. Finally, the simulation results were analyzed and concluded.
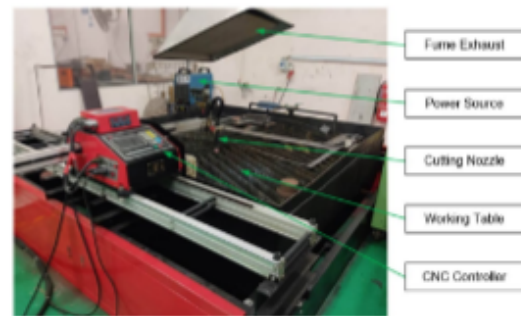

Fig. 1 CNC plasma cutting machine

2 Experimental set-up and procedures

At the initial stage of this research, a series of experiments were conducted using automatic CNC plasma cutting machine model HNC-1500 W with IGBT Inverter power source as displayed in Fig. 1. At the present time, plasma arc cutting process is normally integrated with Computer Numerical Control (CNC) system [26–28]. The implementation of CNC system in plasma cutting process could enhance the cutting flexibility especially to setup and control the torch movement. The type of material used in the experiment was stainless steel 316L with the specimen size of 100 mm in length and width as well as 4 mm in thickness. The cutting parameters applied during the experiment are tabulated in Table 1.

After the experimental cutting process was finished, the specimens were then used for metallographic preparations consisting of several steps prior to final grain size measurement. In preparing the metallographic samples, the specimens underwent sectioning process using abrasive cutter which then proceeded with mounting process by means of automatic mounting press. After finishing mounting process, the samples were subsequently used in crucial course and fine grindings using metallographic sand papers started with lower grade (coarser) and increased gradually to higher grade (finer) by means of grinding machine. Later, polishing process was implemented via polisher machine by utilizing three different grades of polishing agents which were diamond

Table 1 Thermal cutting parameters used for experimental investigation

Parameter	Value
Current, I [A]	30
Voltage, V [V]	80–100
Travel speed, v [mm/s]	5

suspensions of grades 6, 3, and 1 μm. Then, the preparation continued with etching process by using V2A etchant which was suitable for stainless steel material. For better metallographic examination, the inspection of material microstructure was performed just after the etching. The aim of the metallographic inspection was to conduct microscopic examination on the prepared sample in order to measure the grain size at the cut kerf area. The metallographic inspection was carried out using system metallurgical microscope model OLYMPUS BX60F-3. For microscopic measurement, the microscope was connected to a computer equipped with IMAPS 2.0 software. This software program allowed the grain image that was being observed through the microscope to be previewed on the computer which then could be captured and measured. The calculation of real average grain size was made by means of linear intercept method which was performed in accordance to ASTM E112 standard.

According to [29], one of the important parameters to calculate grain size is the modified kinetic constant. However, it is very difficult to find information and reference about the value of this particular parameter. As an alternative to obtain the parameter value, a heat treatment process was conducted using DIL 805A/D/T quenching and deformation dilatometer as shown in Fig. 2. The experiment was carried out on SS316L material in cylindrical shape of 5 mm × 10 mm in diameter and length respectively. A number of samples were heated and held isothermally at four different temperatures of 900 °C, 1000 °C, 1100 °C, and 1200 °C with four different holding times of 30 s, 60 s, 120 s, and 240 s. Based on the results of grain sizes obtained from the heat treatment experiment, the values of modified kinetic constants at each temperature are stated in Table 2. The results of modified kinetic constants are to be implemented in the numerical simulation of grain growth.

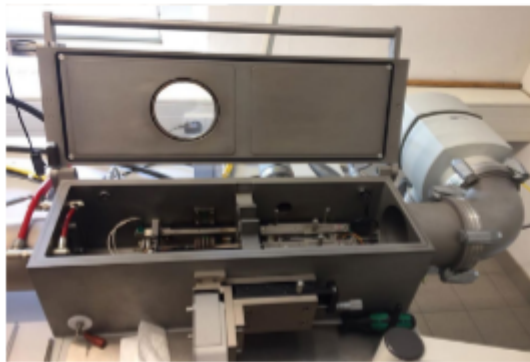Furthermore, a chemical analysis was conducted to identify the composition of chemical substances that were present in the specimen. The chemical testing was performed using QMatrix Analysis by weight percent accomplished based on ASTM A240 specification. Table 3 shows the average results of chemical composition obtained from the experiment and compared with the chemical composition provided in material model from database.

Other factor that might contribute to the accuracy of numerical prediction is the heat transfer coefficient. For this reason, a thermal calibration was conducted in order to ensure the predicted temperature distribution resembling the actual behavior. As calibrating purpose, temperature distribution during the thermal cutting test was measured by means of thermocouples type-K connected to data logger ALMEMO 2890–9 for data recording at specific locations as demonstrated in Fig. 3. Table 4 presents the calibrated heat transfer coefficients obtained from the thermal calibration which were further implemented for the grain growth simulation. The thermal calibration was determined by comparing the temperature distributions obtained between simulation and experiment. Apart from that, the calibration was also made to validate that the chosen material property models used in the numerical analysis as shown in Fig. 6 could characterize the similar behavior as the actual material as displayed in Fig. 4.

Table 2 Modified kinetic constant parameters obtained from heat treatment experiment

Temperature [°C]	Value [$\mu m^2 s^{-1}$]
900	2.94×10^{13}
1000	6.79×10^{12}
1100	1.91×10^{12}
1200	3.22×10^{11}

3 Simulation method and procedures

3.1 Geometrical, material, and thermomechanical modelling

Figure 5 illustrates a schematic diagram of solid finite element model implemented in the numerical computation with the dimension of 20 mm (L) × 40 mm (W) × 4 mm (T). The arrow demonstrates the trajectory and direction of cutting. The geometrical model was built using three-dimensional hexahedral element type. In order to have better numerical prediction, the model was constructed using finer elements in the region close to the cutting trajectory.

For numerical simulation, the grain growth analysis was executed by means of material modelling of SS316L generated based on the chemical composition as disclosed in Table 3. The grain growth computation was made based on temperature distribution where non-linear thermomechanical

Fig. 2 Quenching and deformation dilatometer DIL 805A/D/T

Table 3 Chemical composition of SS316L

Material type	Chemical substance							
	C	Cr	Ni	Mo	Mn	Si	S	P
Specimen	0.017	16.760	10.190	2.148	1.475	0.340	0.0067	0.026
Database	0.018	16.630	11.180	2.050	1.570	0.480	0.0020	0.040

Table 4 Calibrated heat transfer coefficients

Type of heat transfer coefficient	Value
Convective, h [W/m^{2}K]	25
Contact, a [W/m^{2}K]	1000
Emissivity, ε	0.6

method was applied for the temperature analysis. Besides, in this study, the numerical computations were accomplished through temperature-dependent material properties as displayed in Fig. 6. In real situation, the specimen is subjected to high temperature throughout the cutting process which particularly could surpass its melting point at the main cutting area. Consequently, the heat will be transmitted via heat-affected zone (HAZ) region and passed on through base metal as well as ended up dissipating into the surrounding environment. Furthermore, this phenomenon leads to changes in magnitudes of certain material properties that are influenced by the temperature changes. Therefore, it is crucial in the numerical prediction to take the temperature-dependent material properties into consideration in order to replicate the actual condition.

The application of constant material properties could result in inaccurate prediction owing to the consideration that could merely be taken on material behavior at room temperature. On the other hand, due to insignificant changes in magnitudes of particular material properties towards the temperature variation, Poisson's ratio and mass density were possibly considered to be constant at 0.3 and 7850 kg/m^3 respectively. This implementation could also permit reduction in computational time without compromising the accuracy of numerical prediction.

For thermal heat transfer, referring to research by [30], the governing equation for transient heat transfer analysis is represented by Eq. (1). In this equation, ρ is density of the material, c is temperature-dependent specific heat capacity, T is temperature vector, Q is thermal load vector (flux), t is time, and V is the spatial gradient operator, whereas x, y, and z are coordinates in the reference system.

In addition, from the equation, $\vec{q}$ is the thermal conductivity vector in which non-linear isotropic Fourier heat flux constitutive equation is used with temperature-dependent properties.

$$\rho c \frac{\partial T}{\partial t}(x, y, z, t) = -\nabla \cdot \vec{q}(x, y, z, t) + Q(x, y, z, t) \quad (1)$$

In this numerical simulation, two types of system interaction between part and environment were considered, namely, mechanical and thermal boundary conditions. Fixed displacement on the nodal points was set up as the mechanical boundary condition. Meanwhile, as thermal boundary condition, the heat losses were taken into consideration in consequences of conduction (contact between two bodies), convection, and radiation. Equations (2), (3), and (4) are used to characterize the heat losses via conduction, convection, and radiation respectively. Referring to these equations, contact heat transfer coefficient, coefficient of convective heat transfer, Stefan Boltzmann's constant, and thermal emissivity are represented by α h, σ, and ε respectively, while T_1 and T_2 are bodies' temperatures, whereas T_s and T_∞ define the surface and ambient temperatures respectively. Thus, for the thermal boundary condition, the total heat losses involved in the computational analysis could be expressed as Eq. (5).

$$q_{cond} = -\alpha(T_1 - T_2) \quad (2)$$

$$q_{conv} = -h(T_s - T_\infty) \quad (3)$$

$$q_{rad} = -\sigma\varepsilon(T_s^4 - T_\infty^4) \quad (4)$$

$$q_{totallosses} = q_{cond} + q_{conv} + q_{rad} \quad (5)$$

Fig. 3 Data logger ALMEMO 2890–9 (left), type-K thermocouples (middle), and measuring point locations (right) used in thermal calibration
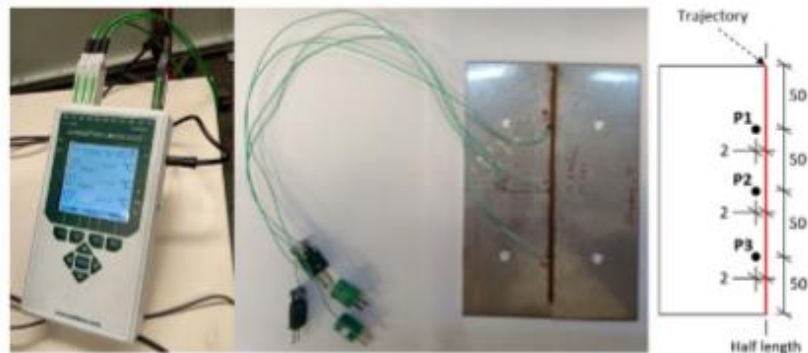
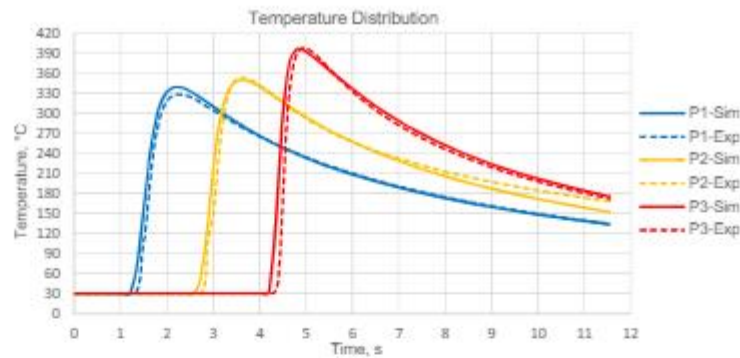Fig. 4 Temperature measurements for thermal calibration

Figure 7 exhibits the basic overview of the coupled thermomechanical-metallurgical analysis. The heat input is defined by the volumetric conical heat source which will be modelled using Fortran-based subroutine and utility routine in FEM software MSC Marc/Mentat 2016.

3.2 Heat source modelling

The application of heat source model is one of the key steps in thermal cutting simulation. The implementation of correct model that is well suited to the simulation process being investigated can give a huge impact on the accuracy of prediction. The heat source model used for simulation should be able to replicate the actual heat source profile. Therefore, in this study, the best preferred model is a volumetric conical heat source model. However, this type of heat source model is usually not provided by default and thus, customized model should be created. Since this simulation is executed using MSC Marc, the algorithm is formulated by means of Fortran-based subroutine. The volumetric conical heat source model implemented throughout this research was developed and formulated in [31] which was exceptionally arisen from derivation of heat intensity distribution from thermal energy conservation equation. The volumetric conical model equation is divided into two parts, where Eq. (6) is generated to characterize the heat intensity distribution of thermal arc while the following Eq. (7) is
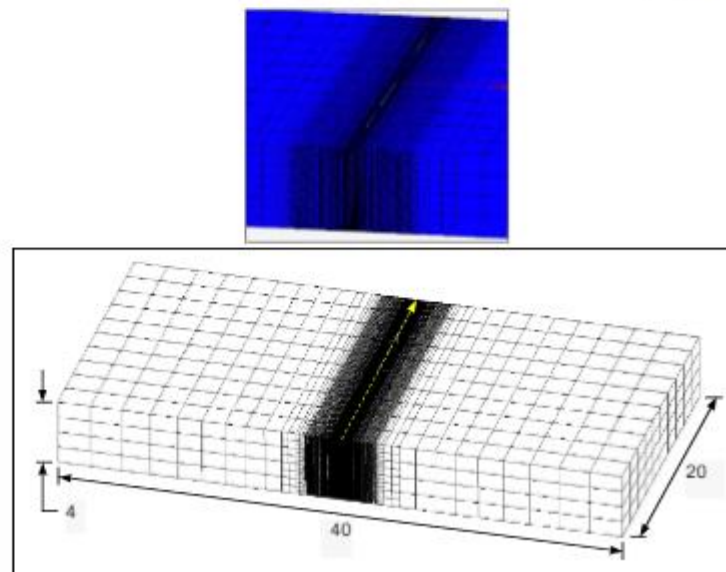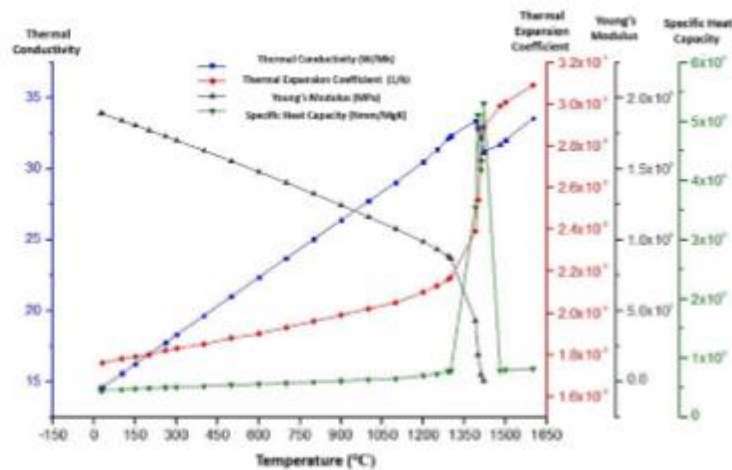
Fig. 5 Geometrical model applied for numerical simulation

Fig. 6 Temperature-dependent mechanical and thermo-physical properties of SS316L.

fraction of the abovementioned equation which manipulates the heat input intensity that deteriorates through the distance of material thickness. Referring to both formulae, the net heat flux, input power, radial coordinate, z-coordinate, and heat intensity distribution parameters are represented by q, Q_o, r, z, and r_o respectively. Meanwhile, r_e and z_e define the top surface radius and z-coordinate respectively, whereas the bottom surface radius and z-coordinate are defined by r_i and z_i respectively. Figure 8 demonstrates the volumetric conical heat source model configuration. The heat source variables applied in the numerical analysis were defined

through the thermal calibration that has been described as above, where the preferred heat source parameters obtained when the predicted temperature distribution could provide the similar behavior of temperature distribution as produced by experiment.

$$q(r,z) = \frac{9Q_o e^3}{\pi (e^3 - 1)} \cdot \frac{1}{(z_e - z_i)(r_e^2 + r_e r_i + r_i^2)} \cdot exp\left(-\frac{3r^2}{r_o^2}\right)$$
(6)

$$r_o(z) = r_i + (r_e - r_i) \cdot \frac{z - z_i}{z_e - z_i}$$
(7)

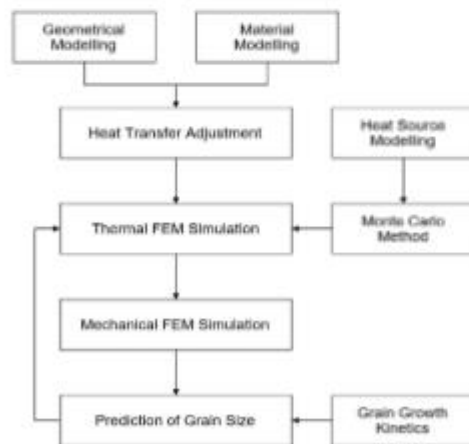### 3.3 Principle of Monte Carlo (MC) method

A numerical model that considers variability of inputs to predict the probable outputs is called MC method, which is also known as probabilistic analysis method. A lot of recalculations could be involved in the numerical analysis prior to finishing. Distributions of different outcome values are possible to be generated via this method. In order to execute the probabilistic analysis, the input powers of heat source energy are fluctuated in a particular range while maintaining the rest of important parameters.

To implement the MC analysis, the input power could be varied through the intervention of random variables. Hence, a source of random variables ought to be generated to implement this process. There are numerous existing random number generators; however, linear congruential generator (LCG) is the most broadly used which can be described as follows [32, 33]:

Fig. 7 The coupled thermomechanical-metallurgical analysis

measurement was lower than both numerical predictions. However, both simulation methods generated good accuracy of prediction where the error percentages were computed below 15%.

6 Conclusions

In conclusion, the analysis of results from this research proved that the grain growth phenomenon occurred as a result of heat input induced in thermal cutting process could possibly be predicted by means of numerical computation. However, the grain growth calculation is not possible to be executed using default numerical analysis. Based on the research findings, the following outcomes derived from this study can be summarized as follows:

- Grain growth prediction is an advanced numerical simulation that could only be performed through customized simulation using particular subroutines. The subroutines involved in this study were the programming codes for conical heat source model which included MC method, contour plotting of desired output, thermal cutting implementation through activation and deactivation of elements, as well as grain size calculation based on Runge–Kutta fourth-order method.
- Based on the numerical analysis, thermal cycle was found to have an impact on the grain growth phenomenon. Furthermore, the reliable calculated grain size obtained from the numerical computation proved that the compiled customized subroutines were successfully implemented to predict the grain growth behavior.
- There were little differences in distributions of grain size estimated through both numerical analyses. However, the probabilistic method predicted closer to the actual grain size value at the specified node as compared to the deterministic method. Therefore, grain growth prediction could be better performed through probabilistic analysis.
- Grain size prediction achieved via probabilistic method provided with higher accuracy in which the percentage of error was less than 10%. Even though the deterministic method ended up with a slightly higher percentage of error, it still managed to provide good prediction with the accuracy of more than 85%.
- The different predictions produced by probabilistic analysis occurred as a result of implementing MC method which considered the variation of input power parameter along the simulation process, where the variation was provided based on normal distribution predicted from the sequence of random numbers that was generated using simple random number generator.
- Moreover, the factors that could lead to result deviations might be caused by chemical composition, material proper-

ties, geometrical size, theoretical model, and approximation method.

Appendix

In this numerical analysis, the subroutine algorithm executed for computing the grain growth can be expressed as follows:

Algorithm 1. Algorithm of metallurgical analysis for calculating grain size.

1:	**procedure** grain size calculation
2:	Set the initial grain size, G0.
3:	Specify the limit temperatures for selecting grain boundary mobility, M0 value.
4:	Assign the parameters of current temp as $\Delta t(1)$ and maximum temp as $\Delta t(3)$.
5:	Assign the parameter of previous grain size as $\Delta t(2)$.
6:	Initialize the grain calculation by setting the starting values for the parameters.
7:	iteration ← 1
8:	**Repeat**
9:	Define the maximum temperature, $\Delta t(3)$.
10:	**if** the current temperature, $\Delta t(1)$ is between temp1 and temp2
11:	Select relevant $M0_1$ by referring to Table 2.
12:	Calculate grain size using Equation (15) based on Equation (14).
13:	**else if** the current temperature, $\Delta t(1)$ is between temp2 and temp3
14:	Select relevant $M0_2$ by referring to Table 2.
15:	Calculate grain size using Equation (15) based on Equation (14).
16:	**else if** the current temperature, $\Delta t(1)$ is between temp3 and temp4
17:	Select relevant $M0_3$ by referring to Table 2.
18:	Calculate grain size using Equation (15) based on Equation (14).
19:	**else if** the current temperature, $\Delta t(1)$ is greater than temp4
20:	Select relevant $M0_4$ by referring to Table 2.
21:	Calculate grain size using Equation (15) based on Equation (14).
22:	**else if** the current temperature, $\Delta t(1)$ is lower than temp1
23:	No grain growth.
24:	**Else**
25:	Grain size is same to the initial size.
26:	**end if**
27:	iteration ← iteration + 1
28:	**until** the maximum number of iterations is completed
29:	**end procedure**

Availability of data and material Not applicable.

Code availability Not applicable.

Declarations

Ethics approval This article does not contain any studies with human participants or animals performed by any of the authors.

Consent to participate Not applicable.

Consent for publication Not applicable.

Conflict of interest All authors declare no competing interests.

References

1. Laitinen A (2015) Two-dimensional simulation of thermal cutting of low-alloyed steels. Tampere University of Technology
2. Abdulateef OF, Mustafa FF, Salman SA (2010) Prediction the effect of flame cutting parameters on the quality of metal surface in CNC flame cutting machine. Iraqi J Mech Mater Eng 10(3):406–416
3. Lindgren LE, Carlestam A, Jonsson M (1993) Computational model of flame-cutting. J Eng Mater Technol Trans ASME 115(4):440–445. https://doi.org/10.1115/1.2904243
4. Niemi J (1985) Teräslevyjen Terminen Leikkaus. Helsinki: Metalliteollisuuden kustannus : Suomen metalliteollisuuden keskusliitto
5. Hendricks BR (1999) Simulation of plasma arc cutting. Peninsula Technikon
6. Prasad GVS, Siores E, Wong WCK (1998) Laser cutting of metallic coated sheet steels. J Mater Process Technol 74(1–3):234–242. https://doi.org/10.1016/S0924-0136(97)00276-8
7. Varkey AP, Kuriakose S, Unni VN (2014) Optimization of edge quality during CO2 laser cutting of titanium alloy. Int J Innov Res Adv Eng 1(11):110–117
8. Bae KY, Yang YS, Yi MS, Park CW (2018) Numerical analysis of heat flow in oxy-ethylene flame cutting of steel plate. Proc Inst Mech Eng Part B J Eng Manuf 232(4):742–751. https://doi.org/10.1177/0954405416654183
9. Arenas MJ, Hömberg D, Lasarzik R, Mikkonen P, Petzold T (2020) Modelling and simulation of flame cutting for steel plates with solid phases and melting," J. Math. Ind., vol. 10, no. 1, 2020, doi: https://doi.org/10.1186/s13362-020-00086-0.
10. Nyon KY, Nyeoh CY, Mokhtar M, Abdul-Rahman R (2012) Finite element analysis of laser inert gas cutting on Inconel 718. Int J Adv Manuf Technol 60(9–12):995–1007. https://doi.org/10.1007/s00170-011-3655-1
11. Kalpakjian S, Schmid SR (2014) Manufacturing engineering and technology, 7th ed. Pearson Education South Asia Pte Ltd
12. Lidam RN, Yupiter HPM, Redza MR, Rahim MR, Sulaiman MS, Zakaria MY (2012) Simulation study on multipassed welding distortion of combined joint types using thermo-elastic-plastic FEM. J Eng Res 9(2):1–16. https://doi.org/10.24200/tjer.vol9iss2pp1-16
13. Mullins JG, Gunnars J (2009) Effect of hardening model on the weld residual stress field in pipe girth welds. In 20th International Conference on Structural Mechanics in Reactor Technology no. SMiRT 20:1–10
14. Arregui-Mena JD, Margetts L, Mummery PM (2014) Practical application of the stochastic finite element method. Arch Comput Methods Eng 23(1):171–190. https://doi.org/10.1007/s11831-014-9139-3
15. Der Kiureghian A, Ke J-B (1988) The stochastic finite element method in structural reliability. Probabilistic Eng Mech 3(2):83–91. https://doi.org/10.1016/0266-8920(88)90019-7
16. Cassidy MJ, Uzielli M, Tian Y (2013) Probabilistic combined loading failure envelopes of a strip footing on spatially variable soil. Comput Geotech 49:191–205. https://doi.org/10.1016/j.compgeo.2012.10.008
17. Liu WK, Mani A, Belytschko T (1987) Finite element methods in probabilistic mechanics. Probabilistic Eng Mech 2(4):201–213. https://doi.org/10.1016/0266-8920(87)90010-5
18. Madić M, Radovanović M, Gostimirović M (2015) ANN modeling of kerf taper angle in CO2 laser cutting and optimization of cutting parameters using Monte Carlo method. Int J Ind Eng Comput 6(1):33–42. https://doi.org/10.5267/j.ijiec.2014.9.003
19. Coll C (2019) Application of probabilistic and deterministic methods for consistent reserves and resources estimation and reporting. In Society of Petroleum Engineers - SPE Europec 81st EAGE Conference and Exhibition pp 1–16. https://doi.org/10.2118/195465-ms
20. Mustaffa Z, van Gelder P, Vrijling H (2009) A discussion of deterministic vs. probabilistic method in assessing marine pipeline corrosions. In Proceedings of the 19th International Offshore and Polar Engineering Conference pp. 653–658
21. Kashyap BP, Tangri K (1992) Grain growth behaviour of type 316L stainless steel. Mater Sci Eng A 149(2):L13–L16. https://doi.org/10.1016/0921-5093(92)90392-E
22. Fujiyama N, Seki A (2018) Austenite grain growth simulation in welding heat-affected zone. Mater Sci Forum 941(2):620–626. https://doi.org/10.4028/www.scientific.net/MSF.941.620
23. Moysan J, Apfel A, Corneloup G, Chassignole B (2003) Modelling the grain orientation of austenitic stainless steel multipass welds to improve ultrasonic assessment of structural integrity. Int J Press Vessel Pip 80(2):77–85. https://doi.org/10.1016/S0308-0161(03)00024-3
24. Das D, Pratihar DK, Roy GG (2018) Cooling rate predictions and its correlation with grain characteristics during electron beam welding of stainless steel. Int J Adv Manuf Technol 97(5–8):2241–2254. https://doi.org/10.1007/s00170-018-2095-6
25. Wang Y, Ding M, Zheng Y, Liu S, Wang W, Zhang Z (2016) Finite-element thermal analysis and grain growth behavior of HAZ on argon tungsten-arc welding of 443 stainless steel. Metals (Basel) 6(77):1–16. https://doi.org/10.3390/met6040077
26. Asiabanpour B, Vejandla DT, Jimenez J, Novoa C (2009) Optimising the automated plasma cutting process by design of experiments. Int J Rapid Manuf 1(1):19–40. https://doi.org/10.1504/ijrapidm.2009.028930
27. Keraita JN, Kim K-H (2007) PC-based low-cost CNC automation of plasma profile cutting of pipes. ARPN J Eng Appl Sci 2(5):1–7
28. Liza FP, Yao CB, Luces JL, Manabat VBE, Baldovino RG (2015) Development of a low-cost controller for the 3-axis computer

numerically-controlled (CNC) plasma cutting machine. Proceedings of the World Congress on Engineering and Computer Science 1:372–376

29. Grong Ø (1997) Metallurgical modelling of welding, Second. The Institute of Materials

30. Attarha MJ, Sattari-Far I (2011) Study on welding temperature distribution in thin welded plates through experimental measurements and finite element simulation. J Mater Process Technol 211(4):688–694. https://doi.org/10.1016/j.jmatprotec.2010.12.003

31. Wu CS, Wang HG, Zhang YM (2006) A new heat source model for keyhole plasma arc welding in FEM analysis of the temperature profile. Weld J 12:284–291

32. Click TH, Liu A, Kaminski GA (2011) Quality of random number generators significantly affects results of Monte Carlo simulations for organic and biological systems. J Comput Chem 32:513–524. https://doi.org/10.1002/jcc.21638

33. Durst MJ (1989) Using linear congruential generators for parallel random number generation. In Proceedings of the 1989 Winter Simulation Conference 53(9):462–466

34. Thistleton WJ, Marsh JA, Nelson K, Tsallis C (2007) Generalized Box-Müller method for generating q-Gaussian random deviates. IEEE Trans Inf Theory 53(12):4805–4810. https://doi.org/10.1109/TIT.2007.909173

35. Addaim A, Gretete D, Madi AA (2018) Enhanced Box-Muller method for high quality Gaussian random number generation. Int J Comput Sci Math 9(3):287–297. https://doi.org/10.1504/IJCSM.2018.093153

36. Rodrigues Dias J (2010) A simple generalization of the Box-Muller method for obtaining a pair of correlated standard normal variables. J Stat Comput Simul 80(9):953–958. https://doi.org/10.1080/00949650902839162

37. McGuire MF (2008) Austenitic stainless steels. In Stainless steels for design engineers. Ohio, USA: ASM International, pp 69–78. https://doi.org/10.31399/asm.tb.ahsssta.t53700151

38. Awrejcewicz J (2014) Ordinary differential equations and mechanical systems. Springer International Publishing. https://doi.org/10.1007/978-3-319-07659-1

39. Tsitouras C (2002) Explicit Runge-Kutta pairs appropriate for engineering applications. Appl Math Model 26:77–88

40. Anak Jutang AS, Razali N, Othman H, Hishamuddin H (2020) Draining of water tank using Runge-Kutta Methods. Int J Recent Technol Eng 8(5):2342–2348. https://doi.org/10.35940/ijrte.e5843.018520

41. Nirmala V, Parimala V, Rajarajeswari P (2018) Application of Runge-Kutta method for finding multiple numerical solutions to intuitionistic fuzzy differential equations. J Phys Conf Ser 1139(1):1–8. https://doi.org/10.1088/1742-6596/1139/1/012012

42. Junior CF, Silva GS, Mendes PS, Machado VA, Ribeiro BN (2018) Implementation of numerical methods of Euler and Runge-Kutta through MATLAB software for the solution of ordinary differential equations dedicated to teaching. Int J Eng Res Appl 8(5):24–29. https://doi.org/10.9790/9622-0805022429

43. Young T, Mohlenkamp MJ (2020) Introduction to numerical methods and MATLAB programming for engineers. Department of Mathematics, Ohio University, Athens, Ohio